Electronic Supplementary Material (ESI) for Journal of Materials Chemistry B.

Supplementary Information

Differential sub-cellular processing of single-wall carbon nanotubes via interfacial modifications

Brian D. Holt,[a] Kris Noel Dahl,[b,c,]* and Mohammad F. Islam[a,]*

[a]Department of Materials Science and Engineering, [b]Department of Biomedical Engineering, [c]Department of Chemical Engineering, Carnegie Mellon University, 5000 Forbes Avenue, Pittsburgh, Pennsylvania 15213-3815, USA

*Corresponding authors: mohammad@cmu.edu, krisdahl@cmu.edu

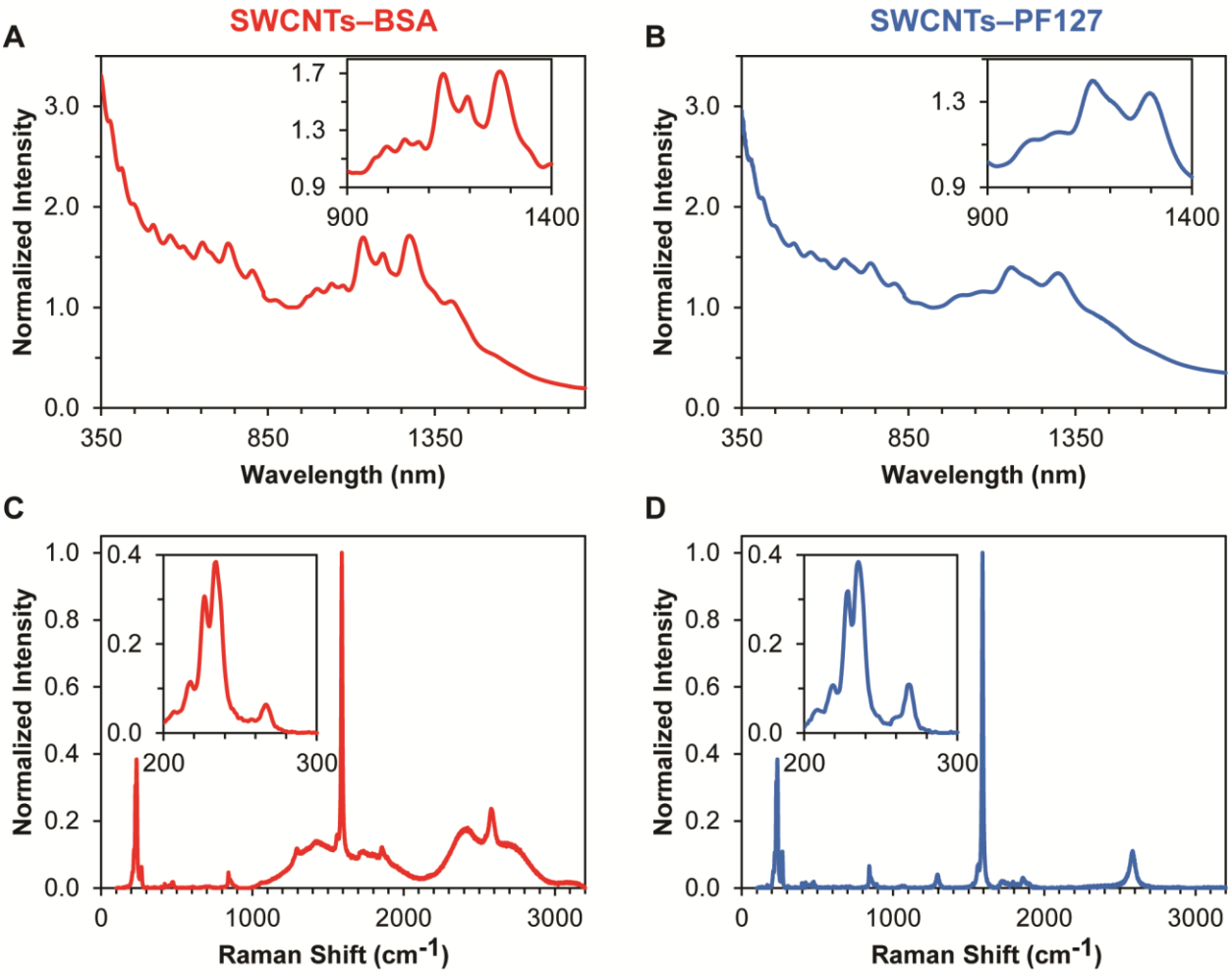

Fig. S1 Materials characterization of SWCNTs. UV–vis–NIR absorbance spectroscopy of (A) SWCNTs–BSA and (B) SWCNTs–PF127 normalized to their absorbance at 930 nm from which SWCNT concentration can be determined using an absorbance coefficient of 2.6 (absorbance · mL) / (mg · mm) for un-normalized data. Insets enlarge the E_{11} region. Peaks arose form van Hove singularities of the density of states and qualitatively indicate SWCNT dispersion quality.[1,2] Raman spectroscopy of (C) SWCNTs–BSA and (D) SWCNTs–PF127 showed characteristic Raman features of SWCNTs including the G-band at ~1591 cm^{-1}.[1] Insets enlarge the radial breathing modes. The broad peaks between ~1000 – ~3000 cm^{-1} in the spectrum for SWCNTs–BSA are contributions from the near-infrared fluorescence of SWCNTs and indicate the presence of pristine, individualized SWCNTs.[1,3] E_{laser} = 1.58 eV (or 785 nm).

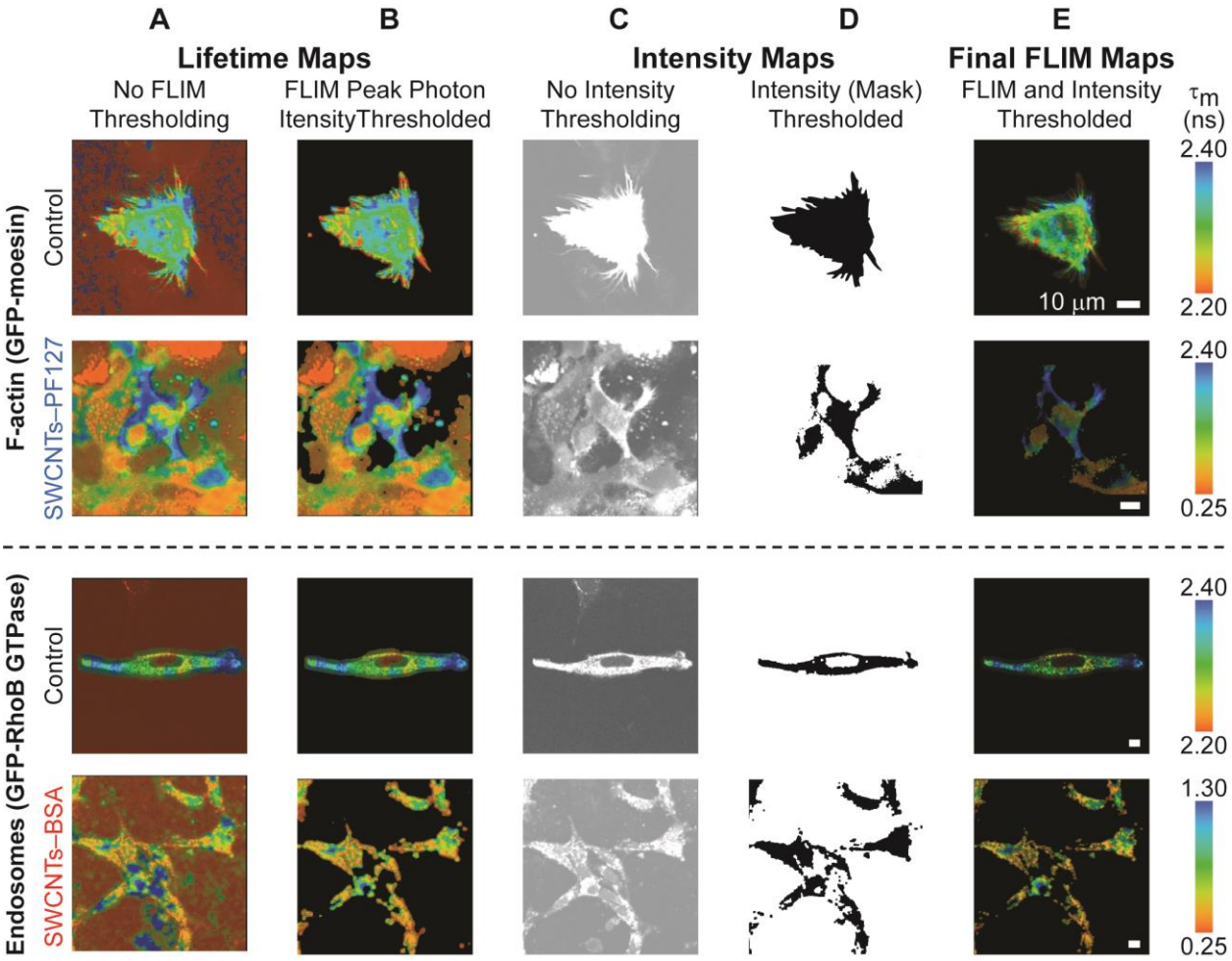

Fig. S2 FLIM image processing. (A) Without any thresholding in the FLIM analysis software (SPCImage, Becker & Hickl), a fluorescence lifetime decay curve was calculated for every pixel, regardless of how many photons were acquired. (B) By setting a minimum peak photon count threshold, most noise was excluded from analysis: extracellular noise pixels that were included in (A) (possess color) but were excluded in (B) (black). Note that FLIM peak photon intensity thresholding was critical as not only did it remove noise from regions which were overtly noise but also its lower limit on peak photon counts ensured that both single and double exponential decays could be validly calculated form the acquired photons.[4,5] (C) The fluorescence intensity image was thresholded (D) in ImageJ to make a mask. Note that for images with a strong signal-to-noise ratio, FLIM-based peak photon count thresholding was sufficient to properly process the images. (E) The final image was thresholded by both the FLIM peak photon count and the intensity mask. Note that only the pixels that were included in the final thresholded image were used for the calculation of average fluorescence lifetimes. All scale bars are 10 μm.

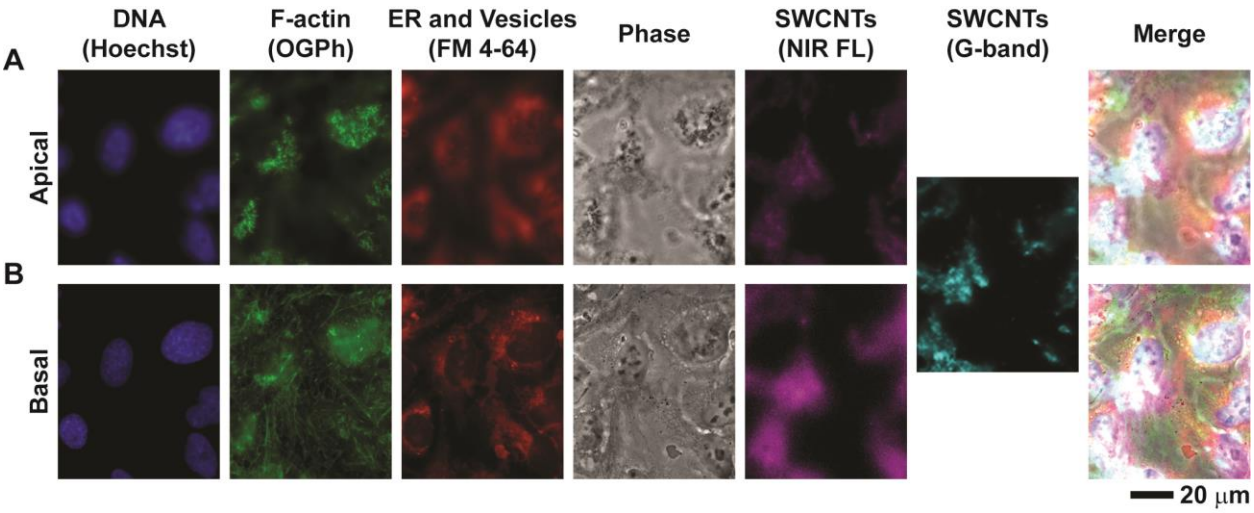

Fig. S3 Apical and basal images of HeLa cells exposed to 50 μg/mL of SWCNTs–PF127, as shown in Fig. 1. (A) Apical images were acquired by focusing the high-resolution widefield microscope on the apical region of the cells. Note the intense fluorescence of F-actin which co-registers with SWCNTs–PF127. (B) Basal images were acquired by focusing on the basal regions of the cells, which typically resulted in well-focused nuclei, cortical and stress fiber F-actin images and well-focused phase images. Raman imaging was not acquired in confocal mode to maximize signal but, consequentially, resulted in less sensitivity to Z-position. Therefore, we only acquired one set of Raman data that represented the intensity of SWCNTs–PF127 throughout the cells. At least 10 cells were imaged in total.

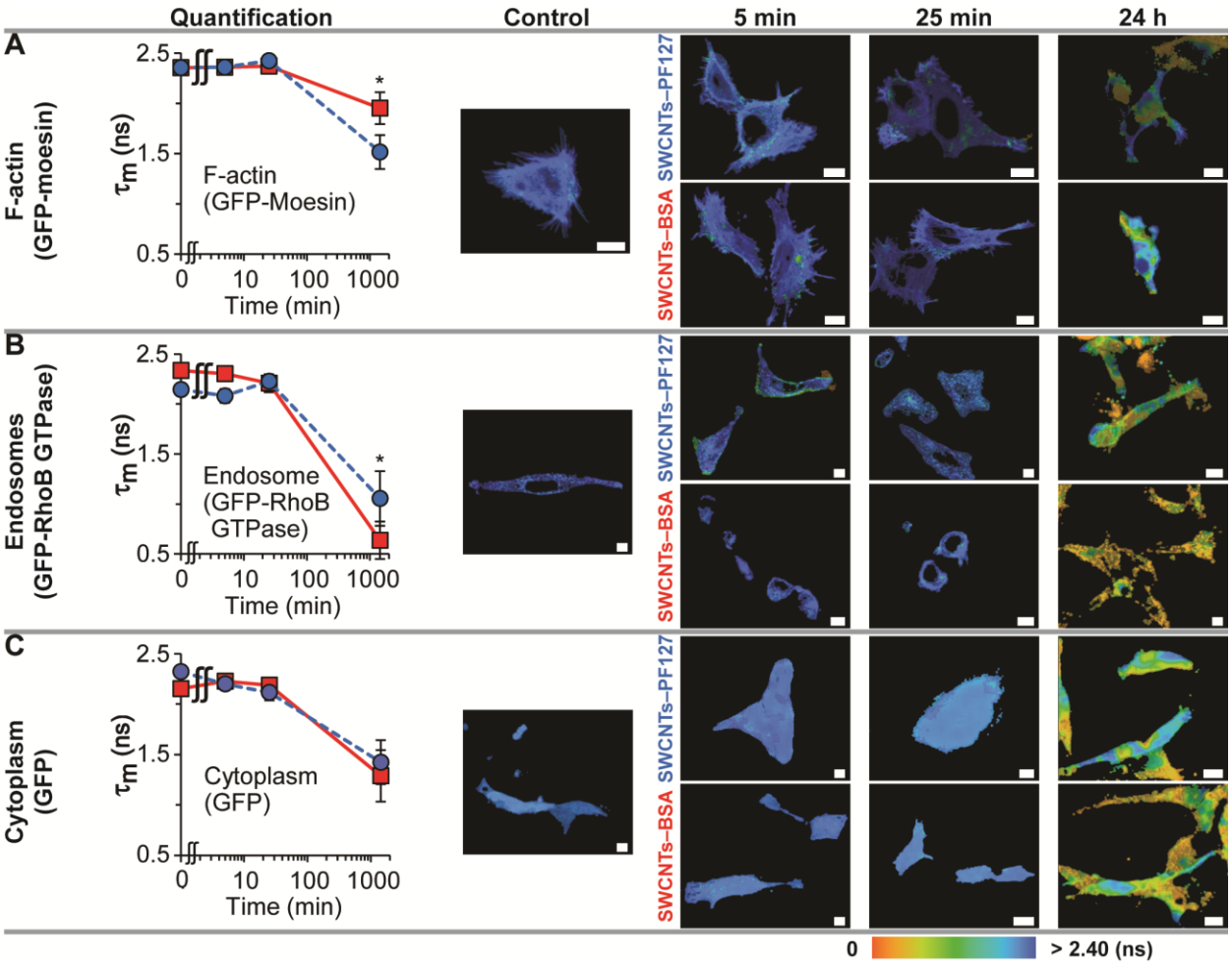

Fig. S4 Quantitative comparison of the average τ_m of GFP-tagged sub-cellular compartments for the indicated time of cellular exposure to 50 μg/mL of SWCNTs–PF127 or SWCNTs–BSA. (A) GFP-moesin that labeled F-actin. (B) GFP-RhoB GTPase that labeled endosomes. (C) GFP that labeled cytoplasm. The number of fields of view for each data point is ≥ 3, and the number of cells for each data point is ≥10. Data points are the average for all fields of view of the average value of τ_m for each field of view. Error bars are standard deviation for each field of view propagated to the final average, and * indicates statistical significance between SWCNTs–PF127 and SWCNTs–BSA at that time point ($p < 0.05$).

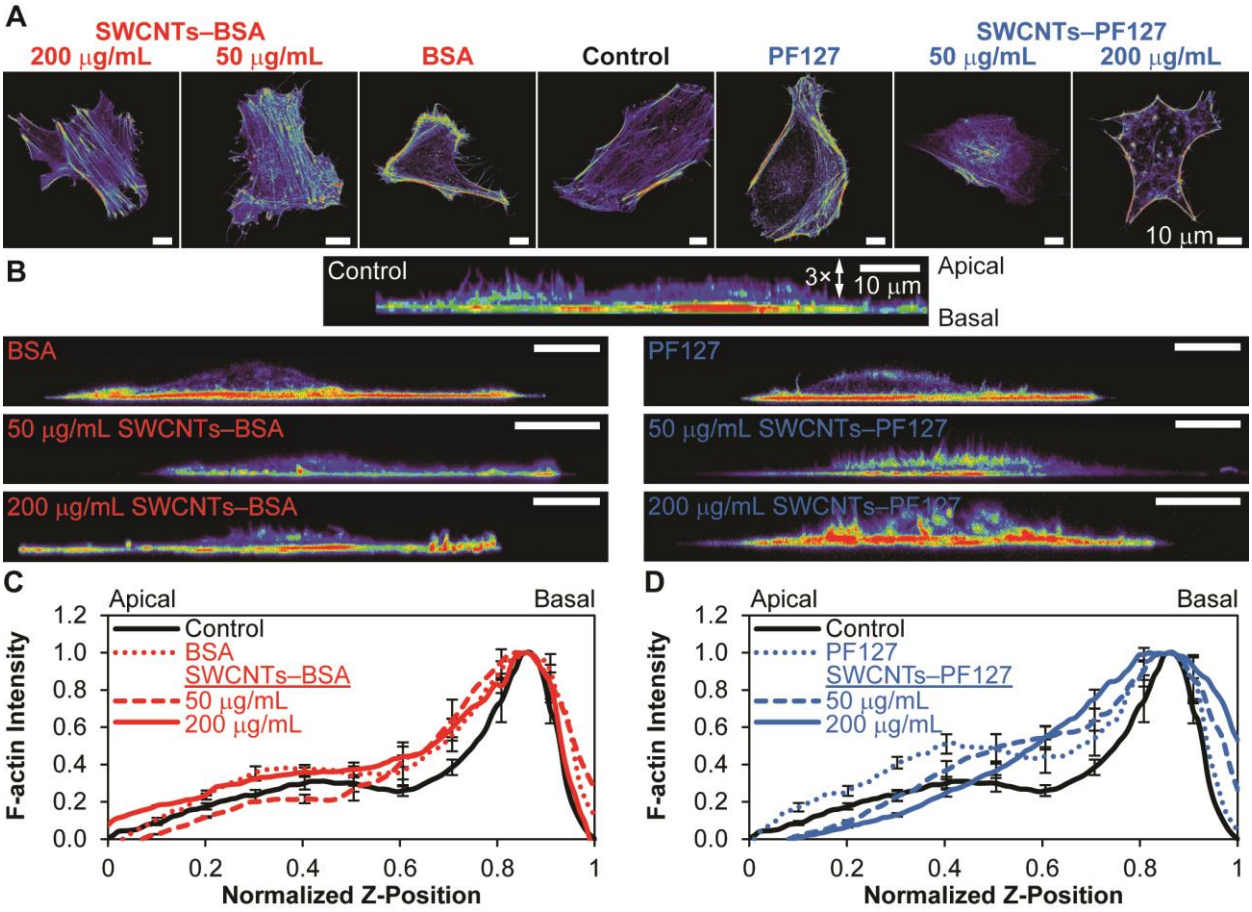

Fig. S5 Confocal fluorescence images and analysis of F-actin of HeLa cells exposed to SWCNTs–PF127 or SWCNTs–BSA for 24 h. (A) Confocal X–Y heat maps compressed in the Z-direction of the fluorescence intensity of Oregon Green 488 phalloidin that labeled F-actin. HeLa cells exposed to SWCNTs–PF127 showed a dose-dependent increase in the alterations of F-actin structures while cells exposed to SWCNTs–BSA showed minimal changes to F-actin distribution. (B) Confocal X–Z heat maps compressed in the Y-direction of the fluorescence intensity of Oregon Green 488 phalloidin that labeled F-actin. HeLa cells exposed to SWCNTs–PF127 showed an increase in the reorganization of apical F-actin structures while cells exposed to SWCNTs–BSA had little change to the distribution of F-actin along the Z-direction. (C,D) Quantification of the Z-distribution of F-actin intensity inside HeLa cells. Multiple X–Z images were scaled across Z-position from where the intensity per pixel was 10% of the maximum both apically and basally and normalized over the domain of [0,1]. Then, the averages for each exposure condition were calculated, normalized to their maxima and the peak intensities were offset to occur at the peak location of the control. The quantified result for HeLa cells exposed to BSA, 50 μg/mL of SWCNTs–BSA and 200 μg/mL of SWCNTs–BSA had very similar profiles to control. The distribution for cells exposed to PF127 was also similar to control. However, cells exposed to SWCNTs–PF127 possessed a dose-dependent increase in altered apical F-actin structures, and the quantification of the fluorescence intensity of F-actin for cells exposed to SWCNTs–PF127 compared to control revealed a decrease of the distinct, concave down peak of F-actin intensity at ~0.4 that likely corresponds to the perinuclear actin cap.[6] Scale bars are all 10 μm; error bars are standard error of the mean. $n = 4$ for control and $n \geq 6$ for all other conditions.

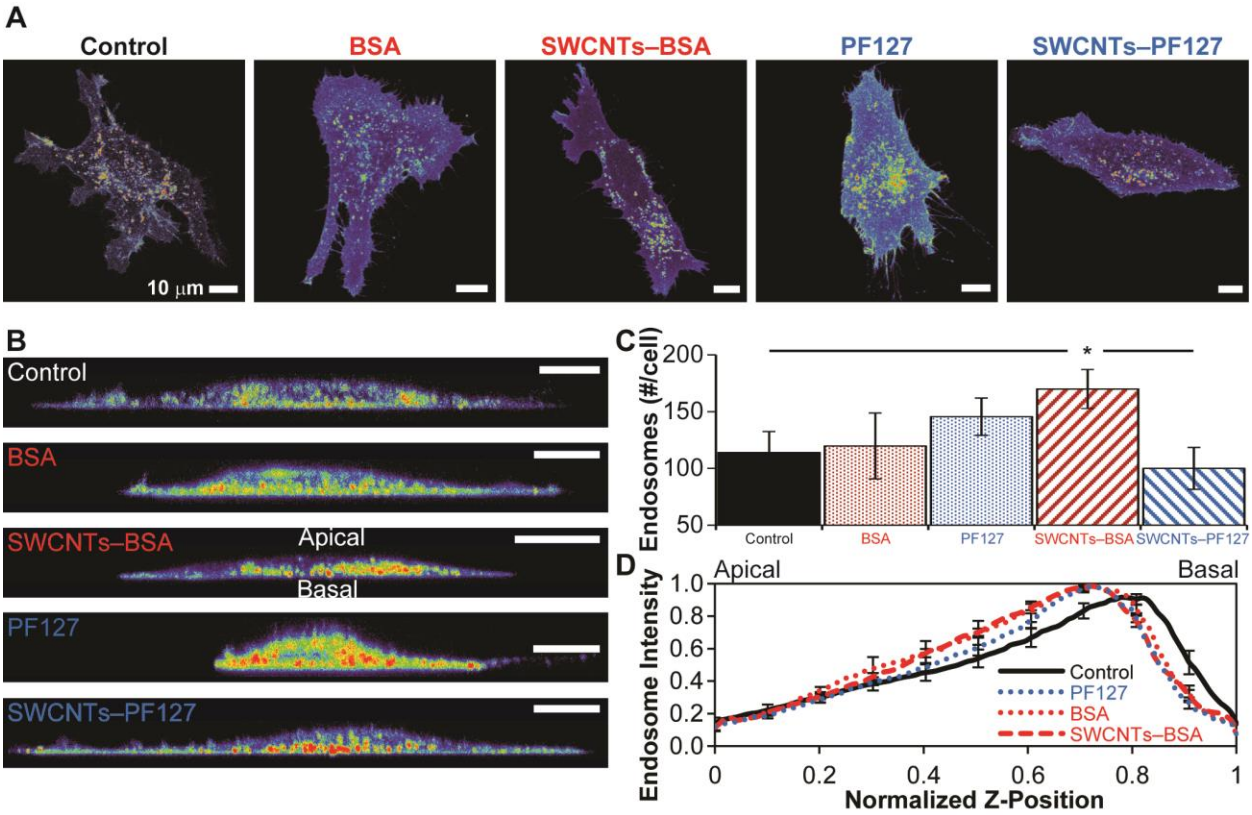

Fig. S6 Confocal fluorescence images and analysis of HeLa cells transfected with GFP-RhoB GPTase that labeled endosomes. (A) Confocal X–Y heat maps compressed in the Z-direction of the fluorescence intensity of GFP-RhoB GTPase that labeled endosomes. (B) Confocal X–Z heat maps compressed in the Y-direction of the same fields of view as (A) enabled a qualitative depiction of the apical/basal distribution of endosomes within cells. (C) Quantification of the number of endosomes per HeLa cell from confocal X–Y heat maps compressed in the Z-direction revealed that HeLa cell exposure to neither the dispersing agents nor 50 μg/mL of SWCNTs–PF127 altered endosome number per cell. However, HeLa cell exposure to 50 μg/mL of SWCNTs–BSA significantly increased the number of endosomes per cell compared to control and cells exposed to 50 μg/mL of SWCNTs–PF127. (D) Quantification of the average fluorescence intensity per pixel of GFP-RhoB GTPase that labeled endosomes along the Z-direction revealed that HeLa cells exposed to PF127 had little alterations to their distribution of endosomes in the Z-direction compared to control. The distribution of endosomes for cells exposed to BSA was similar to that of cells exposed to 50 μg/mL of SWCNTs–BSA, which possessed a slight apical increase in intensity compared to the distribution of control cells. Note that for the quantification, the fluorescence intensity of each X–Z image was first normalized to its maximum and scaled to the normalized Z-position domain of [0,1] based on where the basal and apical fluorescence intensities were 10% of their maxima. Then, these normalized distributions were averaged together; hence, the average may not reach an intensity value of 1. Scale bars are 10 μm. Error bars are standard error of the mean. $n \geq 5$ for all conditions.

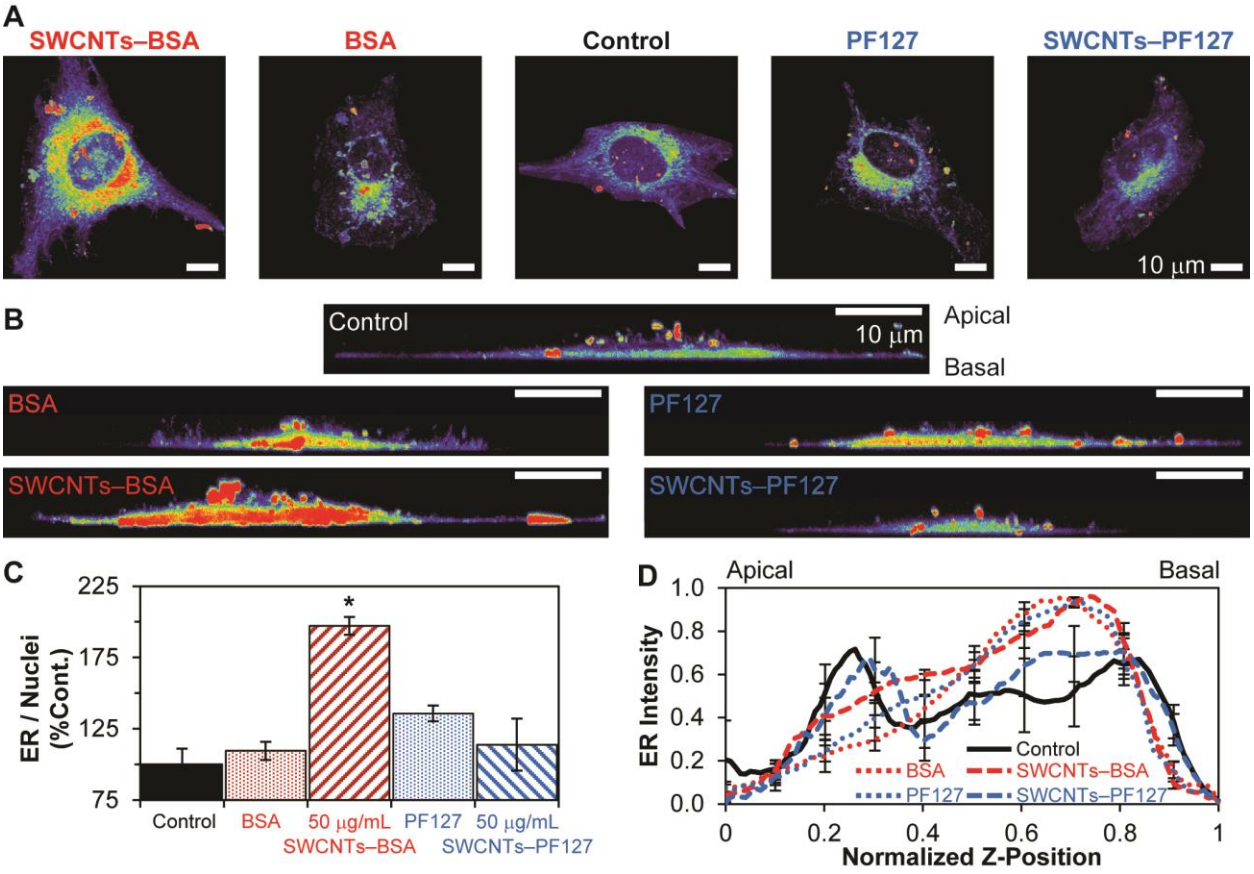

Fig. S7 Redistribution of ER and vesicles. (A) Confocal X–Y heat maps compressed in Z of the fluorescence intensity of FM 4-64 that labeled ER and vesicles. Cells exposed to 50 μg/mL of SWCNTs–BSA had a greater fluorescence intensity of FM 4-64 within cells. (B) Confocal X–Z heat maps compressed in Z of FM 4-64 that labeled ER and vesicles demonstrated that the fluorescence intensity of FM 4-64 was greater in the apical regions of cells exposed to SWCNTs–BSA compared to control. Also, cells exposed to the dispersing agent controls BSA and PF127 possessed a slight increase in the fluorescence intensity of FM 4-64 in the apical regions of the cell. (C) Quantification of the fluorescence intensity of FM 4-64 that labeled ER and vesicles divided by the fluorescence intensity of DAPI that labeled the DNA of HeLa cell nuclei of high-magnification, widefield fluorescence images of HeLa cells statistically confirmed that cellular exposure to SWCNTs–BSA increased the fluorescence intensity of FM 4-64 that labeled ER and vesicles per cell compared to control (* indicates p <0.05). While cellular exposure to BSA or PF127 slightly increased the fluorescence intensity of FM 4-64, it was not a statistically significant increase compared to control. Error bars are standard error of the mean. n >20 fields of view. (D) Quantification of the average fluorescence intensity per pixel of FM 4-64 that labeled ER and vesicles of confocal X–Z images compressed in Z as a function of Z-position revealed that cellular exposure to 50 μg/mL of SWCNTs–PF127 did not alter the Z-direction distribution of ER and vesicles within HeLa cells, but exposure to 50 μg/mL of SWCNTs–BSA slightly altered the Z-direction sub-cellular distribution of ER and vesicles in a manner similar to the distribution for cells exposed to BSA. Error bars are standard error of the mean. n = 5.

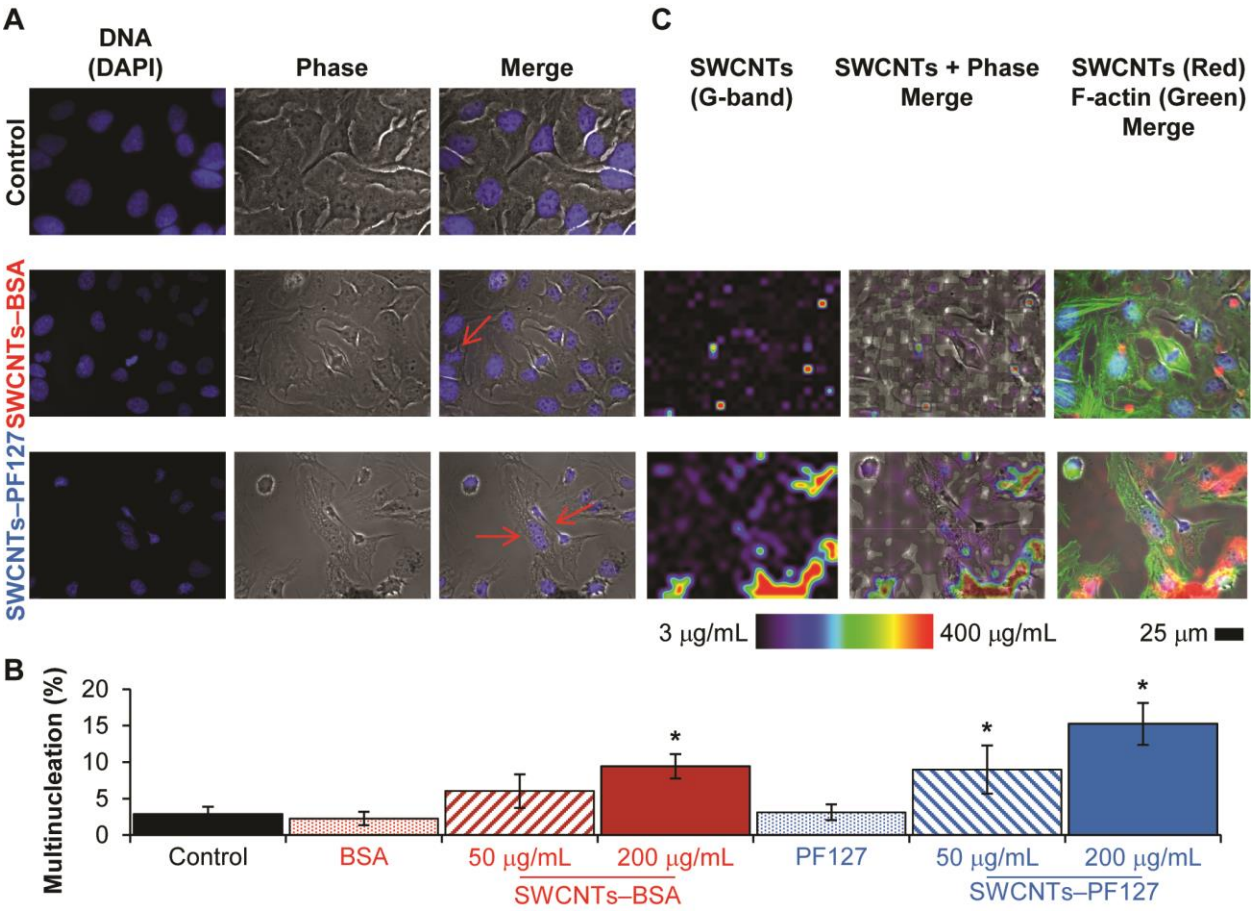

Fig. S8 Multi-nucleation and cellular uptake of SWCNTs. (A) Fluorescence images of DAPI that labeled the DNA of HeLa cell nuclei co-registered to phase contrast images demonstrated that cellular exposure to 200 μg/mL of SWCNTs–BSA or 200 μg/mL of SWCNTs–PF127 induced an increase in multi-nucleation (arrows). (B) Quantification showed a dose-dependent increase in multi-nucleation of HeLa cells exposed to SWCNTs–BSA or SWCNTs–PF127; however, the increased multi-nucleation was more severe for cells exposed to SWCNTs–PF127. Error bars are standard error of the mean. The * indicates statistical significance compared to control using a Bonferroni Correction. $n \geq 275$ for all conditions. (C) Raman mapping of the G-band of SWCNTs showed internalization of SWCNTs within cells. Note that even after multiple wash steps there was a concentrating effect: there were many regions with concentrations at least 2× greater than the exposure concentration of 200 μg/mL. Also, at such high concentrations of SWCNTs–PF127, aggregates of SWCNTs–PF127 were observed on the substrate and associated with cells indicated by the dark regions in phase contrast and areas of high concentration of SWCNTs in the Raman heat maps of the G-band of SWCNTs. Scale bar is 25 μm for all images.

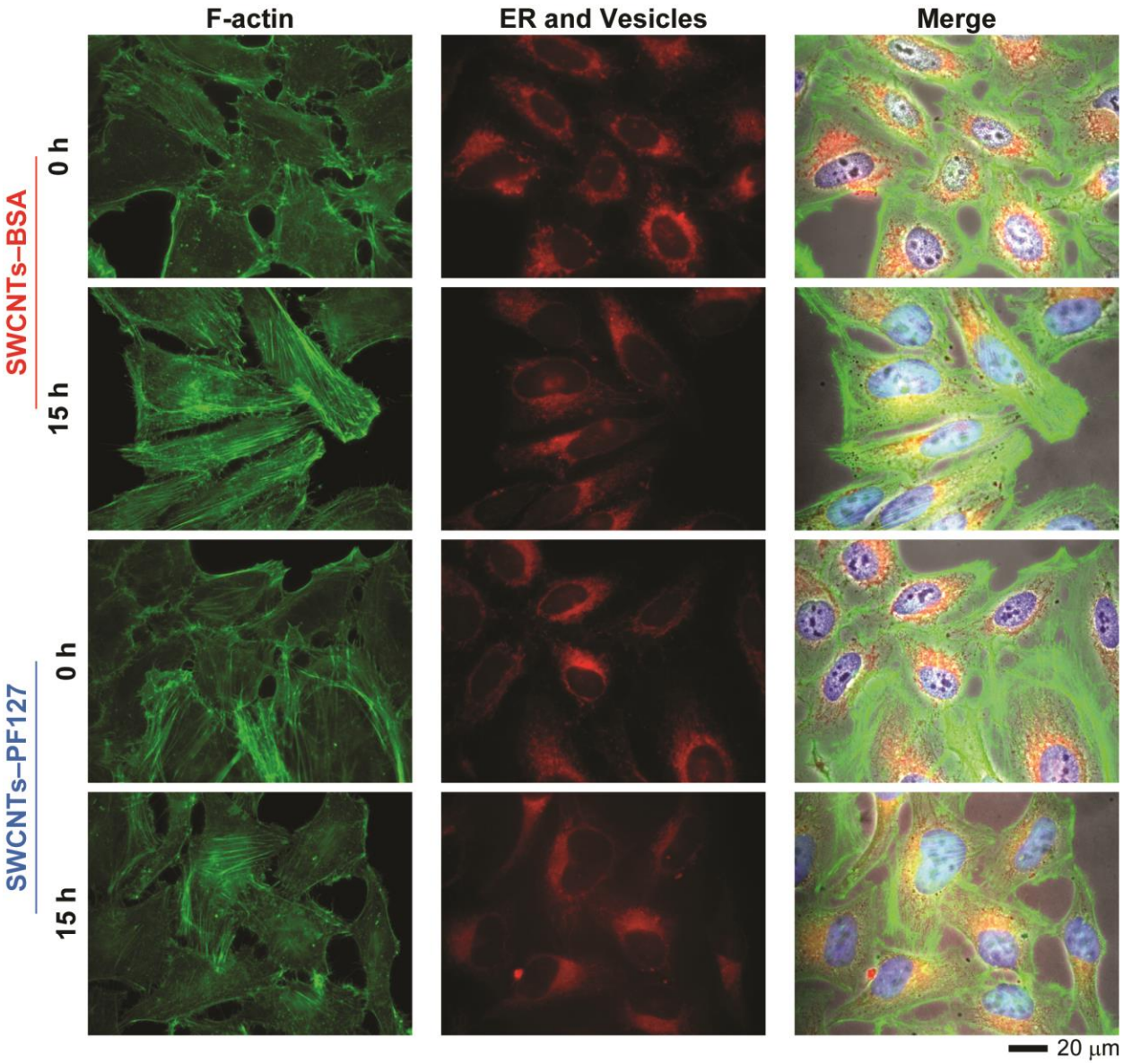

Fig. S9 Images of HeLa cells exposed to 50 μg/mL of SWCNTs–PF127 and the endosome disrupter, chloroquine, as compared to images of HeLa cells that were exposed to 50 μg/mL of SWCNTs–BSA and chloroquine for 4 h. Cells were either immediately fixed, 0 h, or had their SWCNT- and chloroquine-laden media exchanged for fresh, complete cell culture media and allowed to incubate for 15 h. For cells exposed to SWCNTs–PF127, the exposure to chloroquine had little effect on the sub-cellular localizations or fluorescence intensities of cellular compartments, likely because PF127 itself mediated endosome disruption. *n* = 10 fields of view.

References

1 M. S. Dresselhaus, G. Dresselhaus, R. Saito and A. Jorio, *Physics Reports*, 2005, **409**, 47-99.

2 M. J. O'Connell, S. M. Bachilo, C. B. Huffman, V. C. Moore, M. S. Strano, E. H. Haroz, K. L. Rialon, P. J. Boul, W. H. Noon, C. Kittrell, J. P. Ma, R. H. Hauge, R. B. Weisman and R. E. Smalley, *Science*, 2002, **297**, 593-596.

3 B. D. Holt, K. N. Dahl and M. F. Islam, *ACS Nano*, 2012, **6**, 3481-3490.

4 W. Becker, *The bh TCSPC Handbook*, Third edn., 2008.

5 M. Köllner and J. Wolfrum, *Chemical Physics Letters*, 1992, **200**, 199-204.

6 S. B. Khatau, C. M. Hale, P. J. Stewart-Hutchinson, M. S. Patel, C. L. Stewart, P. C. Searson, D. Hodzic and D. Wirtz, *Proceedings of the National Academy of Sciences*, 2009, **106**, 19017-19022.